Master's Thesis

Secondary-side Compensation Circuit for Inductive Power Transfer System

Shogo Isogai
Program of Information Science and Engineering
Graduate School of Science and Technology
Nara Institute of Science and Technology

Supervisor: Prof. Professor Minoru Okada
Network Systems Lab. (Division of Information Science)

Submitted on March 13, 2020

A Master's Thesis
submitted to Graduate School of Information Science,
Nara Institute of Science and Technology
in partial fulfillment of the requirements for the degree of
MASTER of ENGINEERING

Shogo Isogai

Thesis Committee:

Professor Minoru Okada
(Supervisor, Division of Information Science)
Professor Yuichi Hayashi
(Co-supervisor, Division of Information Science)
Associate Professor Takeshi Higashino
(Co-supervisor, Division of Information Science)
Assistant Professor Quang-Thang Duong
(Co-supervisor, Division of Information Science)

Secondary-side Compensation Circuit for Inductive Power Transfer System*

Shogo Isogai

Abstract

We propose a novel compensation circuit for inductive power transfer (IPT) system which is implemented only at the secondary side. In IPT systems, compensation circuits are implemented to suppress reactive components in the circuit to create large currents, resulting in improved power transfer efficiency and capability. The conventional compensation circuit method requires mounting on both the primary side and the secondary side. In the method using a series resonance capacitor on the primary side, a large current flows transmitting coil when the load is absent. Also, in other schemes, the output depends on the mutual inductance between the transmitting and receiving coils. In the proposed method, the reactive component existing on the transmitter side is also canceled by the proposed receiver-side compensation circuit. And this method can simplify primary side while realizing load-independent constant voltage/current functionality. Furthermore, that output value can be changed independently of the mutual inductance. When expanding the proposed system, it is only necessary to install transmitting coils, so that all the changing conditions can be changed only by modifying the compensation circuit, which is considered to be easy to apply to various applications. In this thesis, we show the design of the secondary-side compensation circuit and confirm its effectiveness by simulation and experiment results.

Keywords:

inductive power transfer, secondary-side compensation circuit, constant voltage, constant current

*Master's Thesis, Graduate School of Science and Technology, Nara Institute of Science and Technology, March 13, 2020.

Contents

List of Figures

List of Tables

1 Introduction

1.1 Background and motivations

In 2007, the Witricity team at the Massachusetts Institute of Technology (MIT) succeeded in wirelessly supplying power to a $60\ W$ bulb at a distance of 2 meters [1]. The main techniques of the experiment are "electromagnetic induction of Faraday" and "resonance", and the technology combining these is called inductive power transfer (IPT) [2]. But since 2007, highly efficient and long distance wireless power transmission is enabled by the IPT system [3]. It is used for various devices from consumer electronics to automatic guided vehicles and the future electric cars [4]- [10].

In IPT systems, compensation circuits are implemented to suppress reactive components in the circuit to create large currents, resulting in improved power transfer efficiency and capability. Four basics topologies; series-series (S-S), series-parallel (S-P), parallel-series (P-S), and parallel-parallel (P-P), have been investigated extensively in open literatures [11] [12]. These topologies require resonant capacitors on transmitting and receinving coil. Series-Parallel (S-P) expresses primary-side compensation circuit - secondary-side compensation circuit, so it shows a series resonant capacitor - a parallel resonant capacitor. Based on these basic schemes, more sophisticated compensation circuits, e.g., LLC-S, CLC-LC, LCC-S, LCC-P, LCC-LCC [13]- [16], have been proposed to achieve practically attractive functionalities, e.g., load-independent constant voltage, constant current or zero phase angle (ZPA), where L is a inductor. However, all of these schemes implement compensation circuits for both primary (transmitter) and secondary (receiver) sides as shown in Fig. 1.1(a).

Therefore, when designing the system, it is necessary to investigate reactance components of circuits on both sides and to design each compensation circuit. Further, in the applications of dynamic charging or wide-area charging, since the wide service area needs to be covered by many transmitting coils, these conventional methods have several disadvantages, mainly because of their requirement for transmitter-side implementation. The first disadvantage is the hassle for making a huge a mount of compensation circuits. The second one is the necessity for carefully designing the circuit elements to deal with cross-coupling among the transmitting coils.

In this thesis, we propose a novel compensation topology, which is implemented only at the secondary side as shown in Fig. 1.1(b). In this method, the reactive component existing on the primary side is also canceled by the proposed secondary-side compensation circuit when the coils are coupled. By not installing a compensation circuit in the transmitting coil, even if a change in the system or an external influence is newly added, designing the system is easy because it is only necessary to redesign the compensation circuit on the receiver side. Coupling between the some transmitting coils can also be thought of as combined coil, which is not complicated.

Furthermore, when the receiver side does not present, the current flowing into transmitter side is suppressed and the magnetic field from its coil is weak because there is connection only a power sourve and a transmitting coil having a large reactance component at transmitter side. This can solve the problem of large current flowing in no-load condition which is faulty with S-S and S-P topology. On the other hand, when the receiver side is present, the reactance of the transmitting coil is canceled by the proposed receiver-side compensation circuit, so that a sufficient current corresponding to the load flows to the transmitting coil. Therefore, complicated sensors are unnecessary because it is automatically switched according to the presence or absence of the receiver side, which leads to simplification of the primary side. In addition, the output voltage/current can be controlled only by changing the compensation circuit.

1.2 Contribution

The main contribution of this research is establishing a design of secondary-side compensation circuit which can achieve load-independent constant voltage/current and control output voltage/current. To this end, we investigate the proposed compensation circuit design using ABCD-parameters. We then perform electromagnetic simulations, followed by experiments to validate the analytic results.

Important conclusions are drawn as follows.

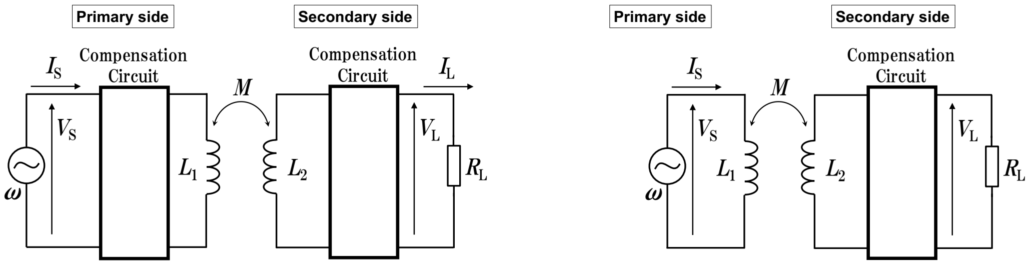

(a) Conventional method (b) Proposed method

Figure 1.1: Inductive power transfer (IPT) system with compensation circuits

1. These verifications show that the output voltage/current can be freely changed only by the secondary-side compensation circuit. Furthermore, their output performance is load independent.

2. This method requires only a power source and a transmitting coil at the primary side. So, This leads to simplification of a complex system using a plurality of power transmitting coils.

1.3 Outline

The remainder of this thesis is organized as follows.

Chapter 2 introduce the IPT system with basic compensation topologies. Chapter 3 investigates the design of the proposed method and further analyzes characteristics in practical conditions. Next, chapter 4 describes EM simulation system which is in various configuration, and show results. Chapter 5 presents experiment setup and shows results. Finally, chapter 6 indicates conclusion and future works.

2 IPT system with basic compensation circuits

In this chapter, we introduce IPT system and its basic compensation circuit. We analyze the characteristics of the four basic compensation topologies; S-S, S-P, P-S, P-P, that are representative of compensation circuit.

2.1 Basic compensation circuits

FIg. 2.1 shows simple equivalent circuit of IPT system with four basic compensation circuit. Here, an internal resistance of the coil is neglected, the values of the transmitting and receiving coil are equal, $L = L_1 = L_2$, and the turns ratio is 1. The power supply is a sinusoidal AC voltage source V_S, and the load is a resistor R_L. A capacitor is inserted in series or in parallel for each compensation method. M is the mutual inductance between the two coils. In this section, we introduce four basic compensation topologies. These methods are adopted to various applications depending on the purpose [17], [18].

2.1.1 S-S compensation topology

In the S-S compensation topology, series capacitors C_{ss1} and C_{ss2} are inserted for primary and secondary side, respectively [19]- [21]. When the capacitor is set to

$$C_{ss1} = C_{ss2} = \frac{1}{\omega^2 L} \tag{2.1}$$

for the resonance angular frequency ω, the output current I_L for the load R_L is

$$I_L = \frac{V_S}{\omega k L}, \tag{2.2}$$

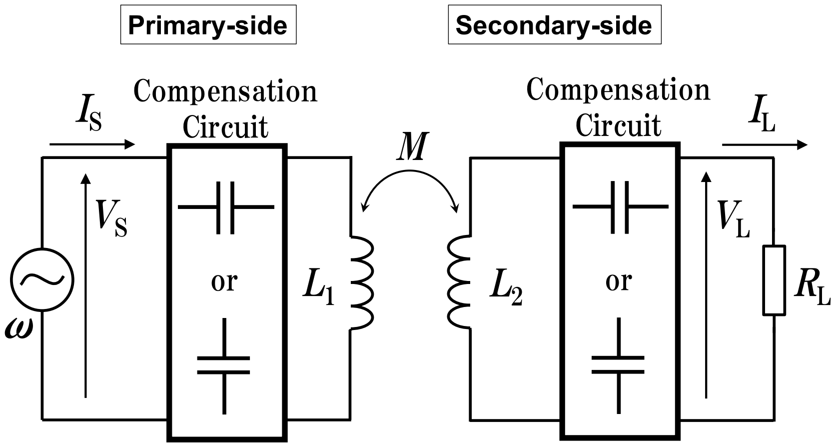

Figure 2.1: Simple equivalent circuit of IPT system with basic compensation circuit

where k is the coupling coefficient between the transmitting and receiving coils,

$$k = \frac{M}{\sqrt{L_1 L_2}}. \tag{2.3}$$

From (2.2), this topology has a load-independent constant current function.

2.1.2 S-P compensation topology

In the S-P compensation topology, a series capacitor C_{sp1} is inserted on the primary side and a parallel capacitor C_{sp2} is inserted on the secondary side [22]- [24]. When the capacitor is set to

$$C_{sp1} = \frac{1}{\omega^2(1-k^2)L_1} \tag{2.4}$$

$$C_{sp2} = \frac{1}{\omega^2 L_2}, \tag{2.5}$$

the output voltage V_L for the load R_L is

$$V_L = \frac{V_S}{k}. \tag{2.6}$$

From (2.6), this topology has a load-independent constant voltage function.

2.1.3 P-S compensation topology

In the P-S compensation topology, a series capacitor C_{ps1} is inserted on the primary side and a parallel capacitor C_{ps2} is inserted on the secondary side [25]- [27]. When the capacitor is set to

$$C_{sp1} = \frac{1}{\omega^2 L_1} \tag{2.7}$$

$$C_{sp2} = \frac{1}{\omega^2 (1-k^2) L_2}, \tag{2.8}$$

the output voltage V_L for the load R_L is

$$V_L = kV_S. \tag{2.9}$$

From (2.9), this topology has a load-independent constant voltage function.

2.1.4 P-P compensation topology

In the P-P compensation topology, parallel capacitors C_{pp1} and C_{pp2} are inserted for primary and secondary side, respectively [28]- [30]. When the capacitor is set to

$$C_{pp1} = C_{pp2} = \frac{1}{\omega^2 (1-k^2) L}, \tag{2.10}$$

the output current I_L for the load R_L is

$$I_L = \frac{kV_S}{\omega (1-k^2) L}. \tag{2.11}$$

From (2.11), this topology has a load-independent constant current function.

2.2 Problem statement

Important problems of these basic compensation topologies are drawn as follows.

1. Four basic topologies require the implementation of a compensation circuit in both the primary and secondary side, which increases the cost and complexity in systems using multiple coils.

2. Series compensation capacitor on the primary side as in S-S and S-P leads to a very large current flowing on the transmitting coil when the secondary-side is absent. This is why that input impedance is very small. Therefore, when using these topologies, On/Off switching mechanism may be required.

3. The output voltage of S-P and P-S topologies having a load-independent constant voltage output function depends on k factor as shown in (2.6) and (2.9).

4. The output current of S-S and P-P topologies having a load-independent constant current output function also depends on k factor as shown in (2.2) and (2.11).

In this work, we propose a novel compensation circuit that solves all of these problems. This compensation circuit is mounted only on the secondary side, and the output can be a constant voltage or a constant current regardless of k factor.

3 Design of secondary-side compensation circuit

In this chapter, we investigate a design of secondary-side compensation circuit which can achieve load-independent constant voltage/current.

3.1 System model

This thesis considers an IPT system with secondary-side compensation circuit shown in Fig. 3.1. Throughout this thesis, it is assumed that all the circuit parameters are linear and that the IPT system is operating in a steady state and includes no switching harmonics. The transmitting coil is connected directly to a voltage source with zero impedance, frequency f and the angular frequency $\omega = 2\pi f$. The receiving coil is connected to a resistive load R_L via a compensation circuit. All the circuit parameters are represented in complex phasor form; specifically, V_S and I_S are the phasors of the fundamental frequency component of the source voltage and current; V_2 and I_2 are the phasors of voltage and current in the receiving coils; V_L and I_L are the phasors of the load voltage and current. In the figure, L_1 is the self inductance of the transmitting coil, L_2 is the self-inductance of the receiving coil, and M is the mutual inductance between the two coils.

In this figure, $\boldsymbol{Z}_x$ represents the Z-paremeters; respectively, $\boldsymbol{Z}_{in}$ is the input; $\boldsymbol{Z}_{ipt}$ is the IPT link as shown in (3.1) ; $\boldsymbol{Z}_{com}$ is the compensation and $\boldsymbol{Z}_L$ is the load resistance.

$$\boldsymbol{Z}_{ipt} = \begin{bmatrix} j\omega L_1 & j\omega M \\ j\omega M & j\omega L_2 \end{bmatrix} \tag{3.1}$$

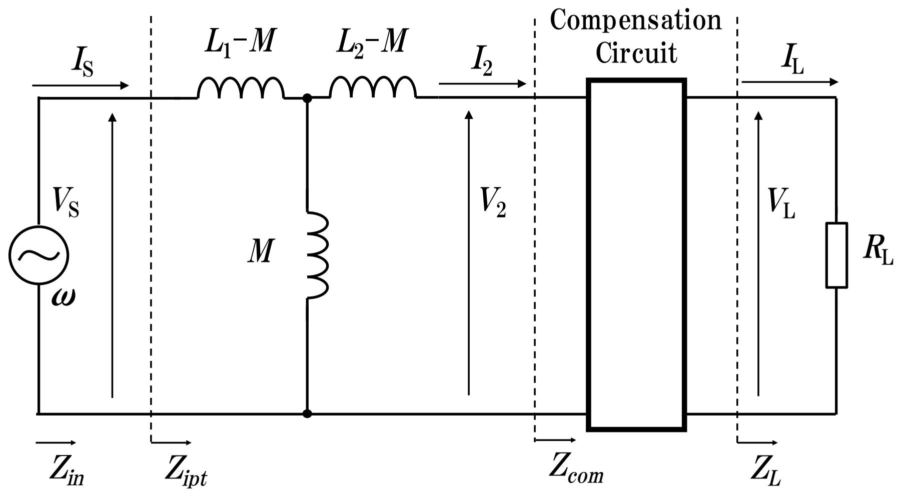

Figure 3.1: Equivalent circuit of IPT system with secondary-side compensation circuit

The input (V_S, I_S) and output (V_2, I_2) relation of the IPT link is characterized by

$$\begin{bmatrix} V_S \\ I_S \end{bmatrix} = \boldsymbol{A}_{ipt} \begin{bmatrix} V_2 \\ I_2 \end{bmatrix}, \tag{3.2}$$

where $\boldsymbol{A}_{ipt}$ is the ABCD-matrix of the IPT link. This matrix can be expressed by

$$\boldsymbol{A}_{ipt} = \begin{bmatrix} \frac{L_1}{M} & \omega(M - \frac{L_1 L_2}{M}) \\ \\ \frac{1}{j\omega M} & \frac{L_2}{M} \end{bmatrix}. \tag{3.3}$$

Let $\boldsymbol{A}_{com}$ be the ABCD-parameters of the compensation circuit, then the voltage and current of the receiving coil are related to those of the load by

$$\begin{bmatrix} V_2 \\ I_2 \end{bmatrix} = \boldsymbol{A}_{com} \begin{bmatrix} V_L \\ I_L \end{bmatrix}. \tag{3.4}$$

As a consequence, the relation between input and output of the whole system is given by

$$\begin{bmatrix} V_S \\ I_S \end{bmatrix} = \boldsymbol{A}_{sys} \begin{bmatrix} V_L \\ I_L \end{bmatrix}, \tag{3.5}$$

where

$$\boldsymbol{A}_{sys} = \boldsymbol{A}_{ipt}\boldsymbol{A}_{com} \tag{3.6}$$

is the ABCD-matrix of the whole system.

3.2 Design of compensation circuit

3.2.1 Constant voltage design

In the constant voltage design, the objective is to yield a stable load voltage V_L for all value of R_L. The target value $V_L^\star$ of the load voltage can be related to the source voltage V_S by a real constant α which represents a transformation ratio. In other words, the parameters $\boldsymbol{A}_{com}$ of the compensation circuit must be chosen so that $V_L^\star = \alpha V_S$ regardless of the value of load current I_L. On the other hand, the target value $I_L^\star$ of the load current must be $I_L^\star = I_S/\alpha$ to achieve unity power factor. As a consequence, the target value for the over all system parameters $\boldsymbol{A}_{sys}^\star$ are determined as

$$\boldsymbol{A}_{sys}^\star = \begin{bmatrix} 1/\alpha & 0 \\ 0 & \alpha \end{bmatrix}. \tag{3.7}$$

Thus, ABCD-parameters of the compensation circuit must be

$$\boldsymbol{A}_{com} = \boldsymbol{A}_{ipt}^{-1}\boldsymbol{A}_{sys}^\star = \begin{bmatrix} \dfrac{L_2}{\alpha M} & j\dfrac{\alpha\omega(M^2 - L_1L_2)}{M} \\ \\ \dfrac{j}{\omega\alpha M} & \dfrac{\alpha L_1}{M} \end{bmatrix}. \tag{3.8}$$

From this it follows that the Z-parameters of the compensation circuit must be equal to

$$\boldsymbol{Z}_{com} = \begin{bmatrix} -j\omega L_2 & -j\omega\alpha M \\ -j\omega\alpha M & -j\omega\alpha^2 L_1 \end{bmatrix}. \tag{3.9}$$

The compensation circuit can be realized by a T-equivalent model shown in Fig. 3.2(a) with capacitors given as below

$$C_1 = \frac{1}{\omega^2(L_2 - \alpha M)} \tag{3.10}$$

$$C_2 = \frac{1}{\omega^2(\alpha^2 L_1 - \alpha M)} \tag{3.11}$$

$$C_3 = \frac{1}{\omega^2 \alpha M}. \tag{3.12}$$

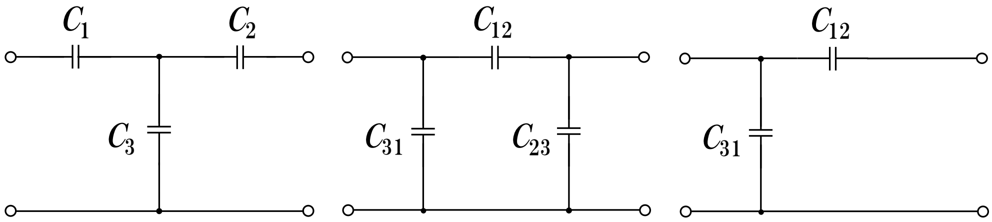

(a) T model (b) π model (c) L model

Figure 3.2: Three type of secondary-side compensation circuit

Or, the compensation circuit can be realized by a π-equivalent model shown in Fig. 3.2(b) with capacitors

$$C_{31} = \frac{\alpha M}{\omega^2 \alpha^2 (L_1 L_2 - M^2)} \tag{3.13}$$

$$C_{12} = \frac{L_2 - \alpha M}{\omega^2 \alpha^2 (L_1 L_2 - M^2)} \tag{3.14}$$

$$C_{23} = \frac{\alpha^2 L_1 - \alpha M}{\omega^2 \alpha^2 (L_1 L_2 - M^2)}. \tag{3.15}$$

Moreover, that can also be realized by a L-equivalent model shown in Fig. 3.2(c). This model is consist of two capacitors $C_{12,31}$ without capacitor C_{23} from the π-equivalent model. We had investigated L-equivalent model paformance in [32].

When the aforementioned compensation circuit is implemented and the ESRs of the coils are ignored, input impedance of the whole system seen by the source is

$$Z_{in} = \frac{1}{\alpha^2} \cdot \frac{V_L^\star}{I_L^\star} = \frac{R_L}{\alpha^2} \tag{3.16}$$

This means the whole system performs an impedance compression on the purely resistive load R_L at a compression ratio of α^2.

3.2.2 Constant current design

In the constant current design, the objective is to yield a stable load voltage I_L for all value of R_L. The target value $I_L^\star$ of the load voltage can be related to the source voltage V_S by a purely imaginary constant $j\beta$ which represents a transformation ratio. In other words, the parameters $\boldsymbol{A}_{com}$ of the compensation circuit must be chosen so that

$I_L^\star = V_S/(j\beta)$ regardless of the value of load voltage V_L. On the other hand, the target value $V_L^\star$ of the load current must be $V_L^\star = j\beta I_S$ to achieve unity power factor. As a consequence, the target value for the over all system parameters $\boldsymbol{A}_{sys}^\star$ are determined as

$$\boldsymbol{A}_{sys}^\star = \begin{bmatrix} 0 & j\beta \\ j/\beta & 0 \end{bmatrix}. \tag{3.17}$$

Thus, ABCD-parameters of the compensation circuit must be

$$\begin{aligned} \boldsymbol{A}_{com} &= \begin{bmatrix} \dfrac{L_2}{M} & j\dfrac{\omega(M^2 - L_1L_2)}{M} \\ \dfrac{j}{\omega M} & \dfrac{L_1}{M} \end{bmatrix} \begin{bmatrix} 0 & j\beta \\ j/\beta & 0 \end{bmatrix} \\ &= \begin{bmatrix} -\dfrac{\omega(M^2 - L_1L_2)}{\beta M} & \dfrac{j\beta L_2}{M} \\ \dfrac{jL_1}{\beta M} & -\dfrac{\beta}{\omega M} \end{bmatrix} \end{aligned} \tag{3.18}$$

From this it follows that the Z-parameters of the compensation circuit must be equal to

$$\boldsymbol{Z}_{com} = \begin{bmatrix} -j\omega(L_2 - \dfrac{M^2}{L_1}) & \dfrac{-j\beta M}{L_1} \\ \dfrac{-j\beta M}{L_1} & j\dfrac{\beta^2}{\omega L_1} \end{bmatrix} \tag{3.19}$$

The compensation circuit can be realized by an equivalent T-model shown in Fig. 3.2(a) with capacitors given as below

$$C_1 = \frac{1}{\omega^2(L_2 - M^2/L_1 - \beta M/\omega L_1)} \tag{3.20}$$

$$C_2 = \frac{1}{\omega^2(-\beta^2/\omega L_1 - \beta M/\omega L_1)} \tag{3.21}$$

$$C_3 = \frac{1}{\beta\omega M/L_1}. \tag{3.22}$$

Or, the compensation circuit can be realized by a π-equivalent model shown in Fig. 3.2(b) with capacitors

$$C_{31} = \frac{\alpha M}{\omega^2\alpha^2(L_1L_2 - M^2)} \tag{3.23}$$

$$C_{12} = \frac{L_2 - \alpha M}{\omega^2\alpha^2(L_1L_2 - M^2)} \tag{3.24}$$

$$C_{23} = \frac{\alpha^2 L_1 - \alpha M}{\omega^2\alpha^2(L_1L_2 - M^2)}. \tag{3.25}$$

When the aforementioned compensation circuit is implemented and the ESRs of the coils are ignored, input impedance of the whole system seen by the source is

$$Z_{in} = \beta^2 \cdot \frac{I_L^\star}{V_L^\star} = \frac{\beta^2}{R_L} \tag{3.26}$$

This means the whole system performs an impedance compression on the purely resistive load β^2 at a compression ratio of R_L.

3.3 Characteristics In Practical Conditions

Taking internal resistances of the coils $r_{1,2}$, the Z-parameters of the IPT link is represented as follows.

$$\boldsymbol{Z}_{ipt} = \begin{bmatrix} r_1 + j\omega L_1 & j\omega M \\ j\omega M & r_2 + j\omega L_2 \end{bmatrix} \tag{3.27}$$

Equivalently, the ABCD-matrix of the IPT link is given by

$$\boldsymbol{A}_{ipt} = \frac{1}{j\omega M}\begin{bmatrix} A_{11}^{ipt} & A_{12}^{ipt} \\ A_{21}^{ipt} & A_{22}^{ipt} \end{bmatrix} \tag{3.28}$$

where

$$\begin{aligned}
A_{11}^{ipt} &= \frac{L_1}{M} + \frac{r_1}{j\omega M} \\
A_{12}^{ipt} &= \frac{(r_1r_2 - \omega^2 L_1L_2 + \omega^2M^2) + j\omega(r_1L_2 + r_2L_1)}{j\omega M} \\
A_{21}^{ipt} &= \frac{1}{j\omega M} \\
A_{22}^{ipt} &= \frac{L_2}{M} + \frac{r_2}{j\omega M}
\end{aligned}$$

3.3.1 Constant Voltage Design

Substituting (3.28) into (3.6), we obtain the end-to-end system's ABCD-matrix as

$$\boldsymbol{A}^{sys} = \begin{bmatrix} A_{11}^{sys} & A_{12}^{sys} \\ A_{21}^{sys} & A_{22}^{sys} \end{bmatrix}, \tag{3.29}$$

where

$$\begin{aligned} A_{11}^{sys} &= 1 + \frac{r_1 r_2}{\omega^2 M^2} + j\frac{r_2 L_1}{\omega M^2} \\ A_{12}^{sys} &= r_1 + r_2\frac{L_1^2}{M^2} - j\frac{r_1 r_2 L_1}{\omega M^2} \\ A_{21}^{sys} &= \frac{r_2}{\omega^2 M^2} \\ A_{22}^{sys} &= 1 - j\frac{r_2 L_1}{\omega M^2} \end{aligned}$$

The ratio of input voltage to output voltage is determined as

$$\begin{aligned} \frac{V_L}{V_S} &= \left|\frac{1}{A + B/R_L}\right| \\ &= \left[\left(1+\frac{r_1 r_2}{\omega^2 M^2}+\frac{r_1 M^2+r_2 L_1^2}{M^2 R_L}\right)^2+\frac{r_2^2 L_1^2}{\omega^2 M^4}\left(1-\frac{r_1}{R_L}\right)^2\right]^{-\frac{1}{2}} \\ &\approxeq \left[\left(1+\frac{r_2\left(\frac{L_1}{M}\right)^2}{R_L}\right)^2+\left[\frac{r_2\left(\frac{L_1}{M}\right)^2}{\omega L_1}\right]^2\left(1-\frac{r_1}{R_L}\right)^2\right]^{-\frac{1}{2}} \end{aligned} \tag{3.30}$$

$$V_S = AV_L + BI_L = (AR_L + B)I_L \tag{3.31}$$

$$I_S = CV_L + DI_L = (CR_L + D)I_L \tag{3.32}$$

In put power is given by

$$P_{in} = \frac{1}{2}\mathrm{Re}\{V_1 I_1^*\} \tag{3.33}$$

$$= \frac{1}{2}\mathrm{Re}\{(AR_L + B)(CR_L + D)^* |I_L|^2\} \tag{3.34}$$

$$= \frac{1}{2}\mathrm{Re}\{(AR_L + B)(C^* R_L + D^*) |I_L|^2\} \tag{3.35}$$

The efficiency is given by

$$\eta = 1/Re\{AC^* R_L + BD^*/R_L + BC^* + AD^*\} \tag{3.36}$$

$$= \frac{1}{1+\frac{2r_1r_2}{\omega^2M^2}+\left(1+\frac{r_1r_2}{\omega^2M^2}\right)\frac{r_2R_L}{\omega^2M^2}+\left(r_1+r_2\frac{L_1^2}{M^2}+\frac{r_1r_2L_1^2}{\omega^2M^4}\right)\frac{1}{R_L}} \tag{3.37}$$

3.3.2 Constant Current Design

Substituting (3.28) into (3.6), we obtain the end-to-end system's ABCD-matrix as

$$\boldsymbol{A}^{sys} = \begin{bmatrix} A_{11}^{sys} & A_{12}^{sys} \\ A_{21}^{sys} & A_{22}^{sys} \end{bmatrix}, \tag{3.38}$$

where

$$\begin{aligned} A_{11}^{sys} &= \frac{r_1r_2L_1}{\omega M^2} + jr_1 + jr_2\frac{L_1^2}{M^2} \\ A_{12}^{sys} &= -\frac{r_2L_1}{\omega M^2} + j + j\frac{r_1r_2}{\omega^2M^2} \\ A_{21}^{sys} &= \frac{r_2L_1}{\omega M^2} + j \\ A_{22}^{sys} &= j\frac{r_2}{\omega^2M^2} \end{aligned}$$

The ratio of input voltage to output voltage is determined as

$$\begin{aligned} \frac{jI_L}{V_S} &= \left|\frac{1}{AR_L + B}\right| \\ &= \left[\frac{r_2^2L_1^2}{\omega^2M^4}\,(R_Lr_1-1)^2+\left(R_L\frac{r_1M^2+r_2L_1^2}{M^2}+\frac{r_1r_2}{\omega^2M^2}+1\right)^2\right]^{-\frac{1}{2}} \\ &\approx \left[\left[\frac{r_2\left(\frac{L_1}{M}\right)^2}{\omega L_1}\right]^2(R_Lr_1-1)^2+\left(1+R_Lr_2\left(\frac{L_1}{M}\right)^2\right)^2\right]^{-\frac{1}{2}} \end{aligned} \tag{3.39}$$

$$V_S = AV_L + BI_L = (AR_L + B)I_L \tag{3.40}$$

$$I_S = CV_L + DI_L = (CR_L + D)I_L \tag{3.41}$$

In put power is given by

$$P_{in} = \frac{1}{2}\mathrm{Re}\{V_S I_S^*\} \tag{3.42}$$

$$= \frac{1}{2}\mathrm{Re}\{(AR_L + B)(CR_L + D)^* |I_L|^2\} \tag{3.43}$$

$$= \frac{1}{2}\mathrm{Re}\{(AR_L + B)(C^* R_L + D^*) |I_L|^2\} \tag{3.44}$$

The efficiency is given by

$$\eta = 1/\mathrm{Re}\{AC^* R_L + BD^*/R_L + BC^* + AD^*\} \tag{3.45}$$

$$= \frac{1}{1+\frac{2r_1r_2}{\omega^2M^2}+\left(\frac{r_1r_2L_1^2}{\omega^2M^4}+r_1+r_2\frac{L_1^2}{M^2}\right)R_L+\left(\left(1+\frac{r_1r_2}{\omega^2M^2}\right)\frac{r_2}{\omega^2M^2}\right)\frac{1}{R_L}} \tag{3.46}$$

4 Simulation Evaluation

We investigate the availability of the design of the secondary-side compensation circuit mentioned in capter 2 by simulation results.

4.1 Simulation setup

We employ WIPL-D©, a commercial EM simulation software based on the method of moments, to evaluate the proposed IPT system shown in Fig. 4.1. In this configuration, the lower coil is the transmitter and the upper coil is the receiver. Both the transmitter and receiver are identical 8-turn spiral coils made of copper wire with a conductivity of $58 \times 10^6\ \mathrm{S/m}$ and a diameter of 1 mm. Self inductances of the coils are $L_1 = 14.35\mu\mathrm{H}$ and $L_2 = 14.35\mu\mathrm{H}$, and their mutual inductance is $M = 6.64\mu\mathrm{H}$. The operating frequency is $2\ \mathrm{MHz}$. Other parameters of the coils can be found in Table 4.1.

4.2 Simulation results

4.2.1 Constant voltage design

With simulation setup values and (3.12) , capacitances of the proposed compensation circuit when α is 0.5, 1 and 2 and input impedance of the whole system at $R_L = 0\ \Omega$ are shown in Table 4.2. It can be confirmed that the reactive components of the system is canceled in all three types of compensation circuits as indicated by (3.16).

Fig. 4.2 demonstrates the ratio of output to input voltage and current at three different α a function of the load resistance R_L. As shown in this figure, this system performs the desired performance of $V_L^{\star} = \alpha V_S$ and $I_L^{\star} = I_S/\alpha$. And as α increases, a larger load is required to stabilize the voltage ratio. However, as α decreases, the current ratio stabilizes over a wide range of the load.

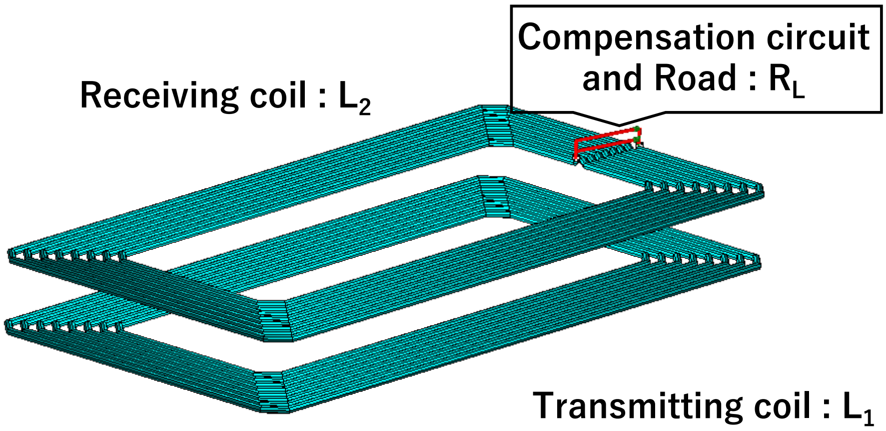

Figure 4.1: Simulation model

Next, Fig. 4.3 shows simulation results of the efficiency at three different α a function of the load resistance R_L. From these results, it can be confirmed that load value at which the efficiency peaks varies and the load range which the efficiency stabilizes differs depending on α.

4.2.2 Constant current design

We prepare a compensation circuit of constant current design under the same conditions as the previously described constant voltage design. With these values, capacitances of the proposed compensation circuit when β is 1, 50 and 100 and input impedance of the whole system at $R_L = 0\Omega$ are shown in Table. 4.2. It can be confirmed that the input impedance increases as β increases, as indicated by (3.26).

Fig. 4.4 demonstrates the ratio of output to input voltage and current at three different β a function of the load resistance R_L. As shown in this figure, only when β is very large, this system performs the desired performance of $I_L^\star = V_S/(j\beta)$ and $V_L^\star = j\beta I_S$. Next, Fig. 4.5 shows simulation results of the efficiency at three different β a function of the load resistance R_L.

Table 4.1: Simulation paramters

Parameters	Value
Operating fequency f	2.0 [MHz]
Coil size	100×200 [mm]
Coil gap d	20 [mm]
Transmitting coil inductance L_1	14.35 [μH]
Internal resistance of transmitting coil r_1	520 [mΩ]
Receiving coil inductance L_2	14.35 [μH]
Internal resistance of receiving coil r_2	520 [mΩ]
Mutual inductance M	6.64 [μH]
Input voltage V_S	12 [V]
Conductivy	58×10^6[S/m]
Copper wire dianeter	1.0 [mm]
Analysis	$moment\ method(MoM)$

Table 4.2: Compensation circuit parameters of constant voltage design and input impedance of whole system in simulation

α	C_1	C_2	C_3	Z_{in}
2.0	574.1 [pF]	23.67 [nF]	1.91 [nF]	$2.46 + j0.28$ [Ω]
1.0	821.2 [pF]	821.2 [pF]	953.0 [pF]	$2.47 + j0.16$ [Ω]
0.5	9.52 [nF]	143.5 [pF]	476.9 [pF]	$2.47 + j0.04$ [Ω]

Table 4.3: Compensation circuit parameters of constant current design and input impedance of whole system in simulation

β	C_1	C_2	C_3	Z_{in}
100	833.7 [pF]	8.09 [μH]	1.71 [nF]	$9869 - j5826$ [Ω]
50	671.0 [pF]	2.94 [μH]	3.43 [nF]	$3599 - j5804$ [Ω]
1.0	563.3 [pF]	367.77 [nH]	171.97 [nF]	$2.55 - j3.36$ [Ω]

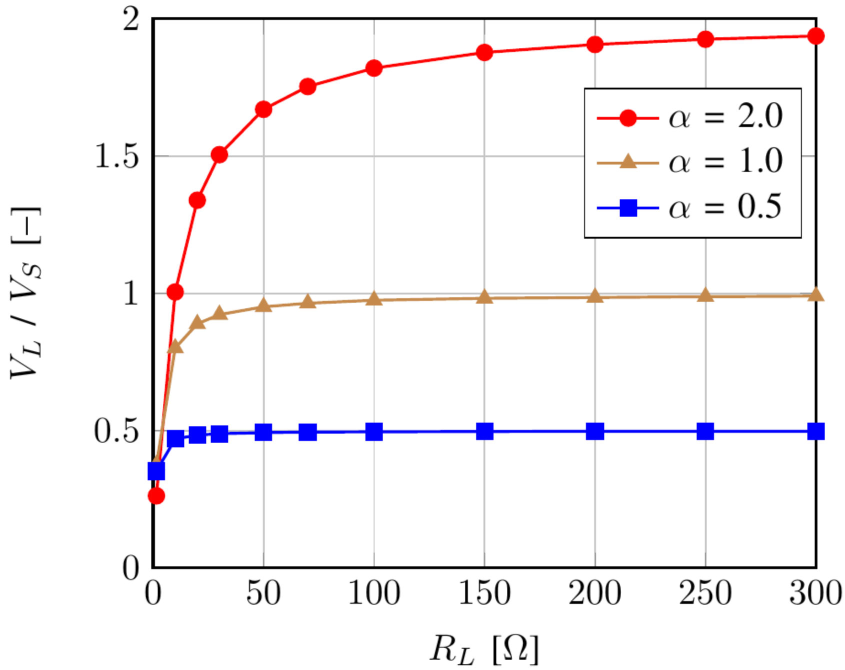

(a) Ratio between source and load voltages

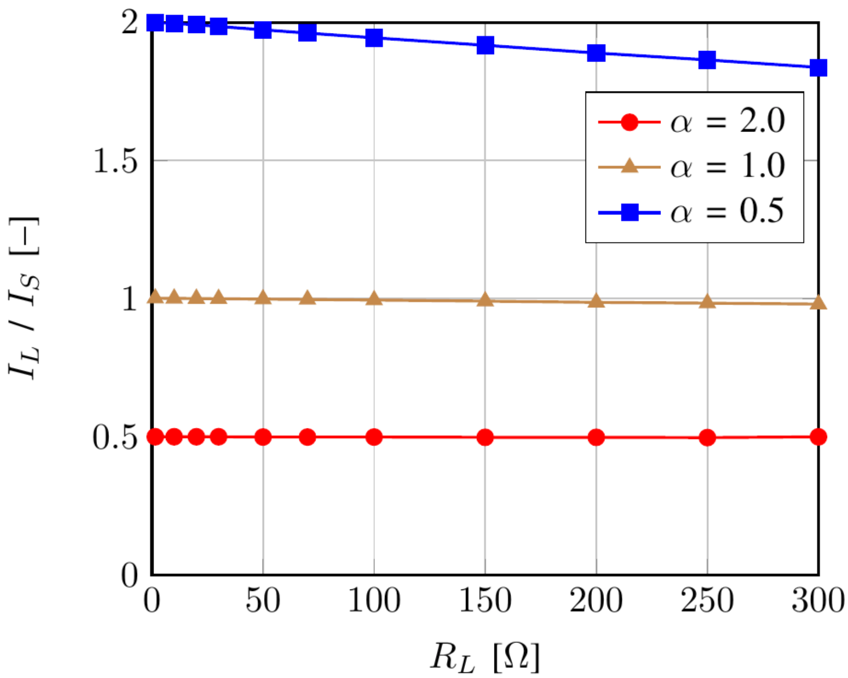

(b) Ratio between source and load current

Figure 4.2: Simulation results for ratio of output to input voltage and current with constant voltage design

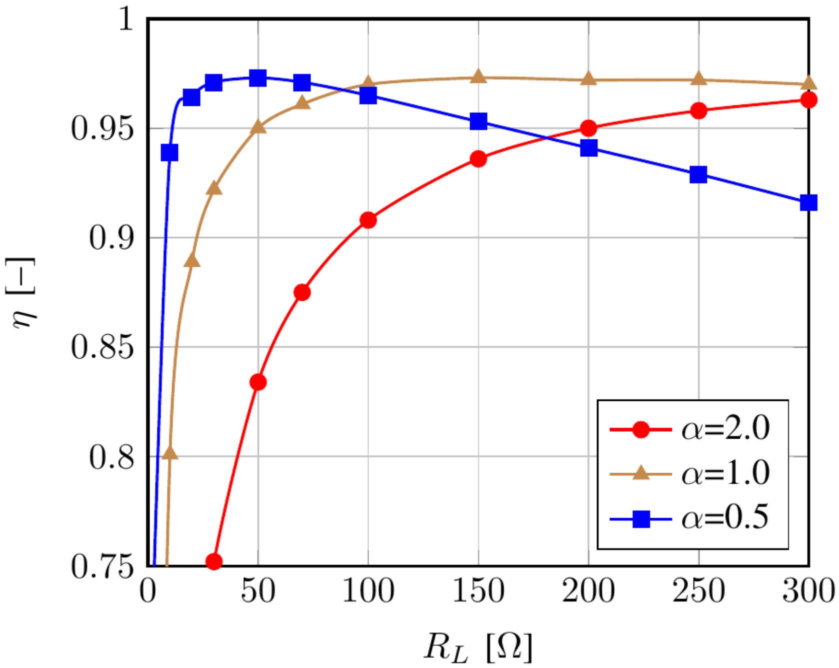

Figure 4.3: Simulation results for efficiency with constant current design

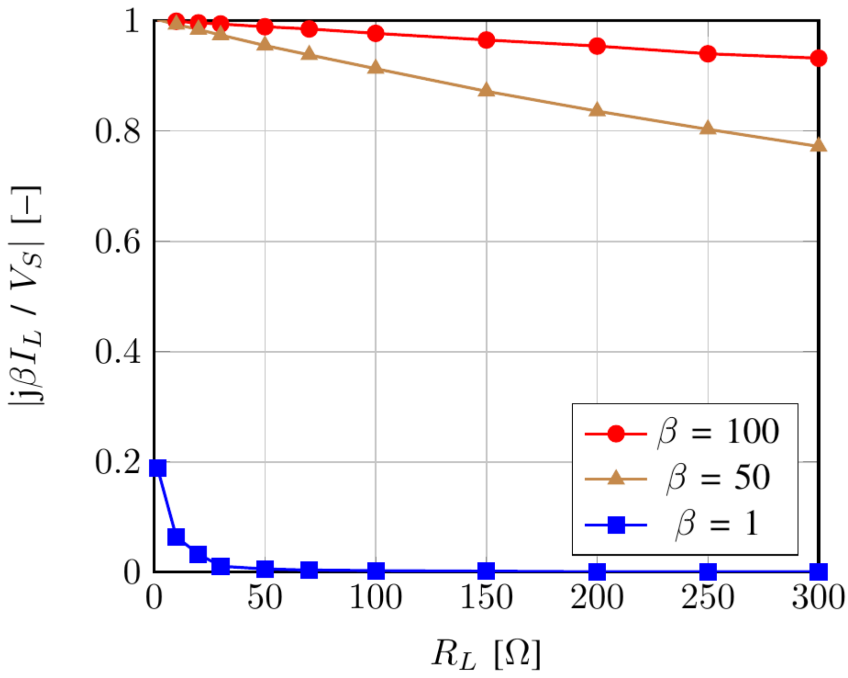

(a) Ratio between source and load current

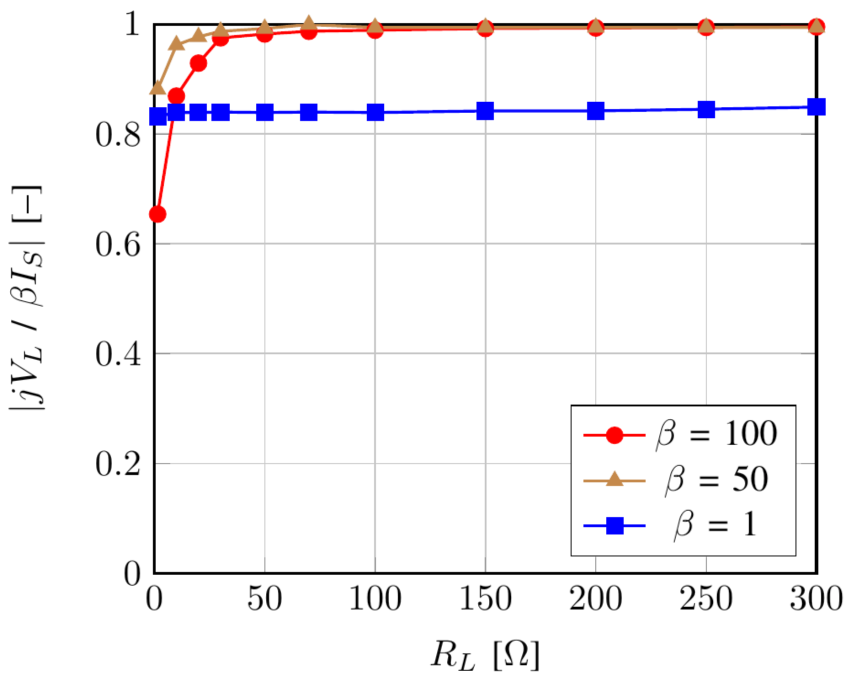

(b) Ratio between source and load voltage

Figure 4.4: Simulation results for ratio of output to input voltage and current with constant current design

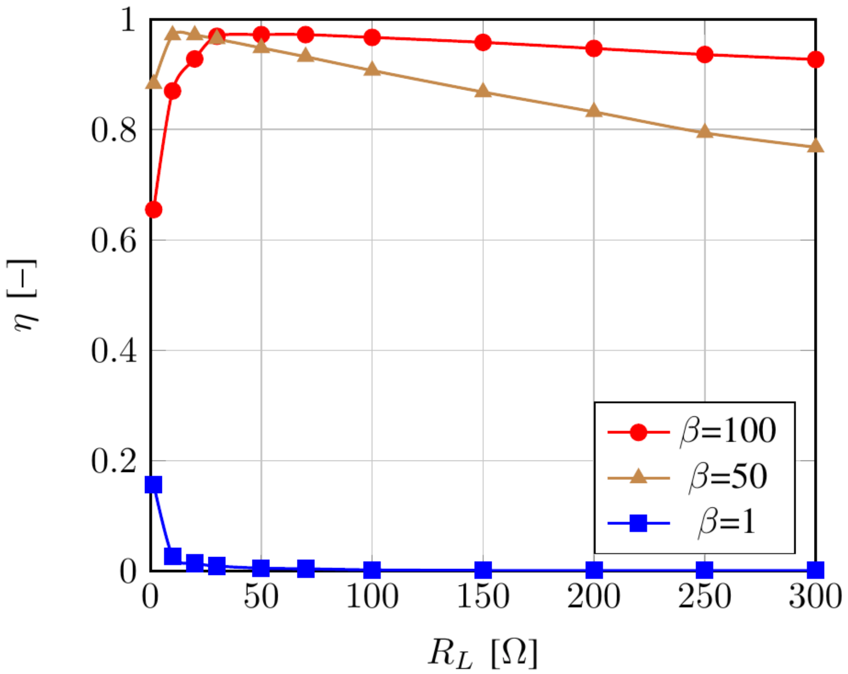

Figure 4.5: Simulation results for efficiency with constant current design

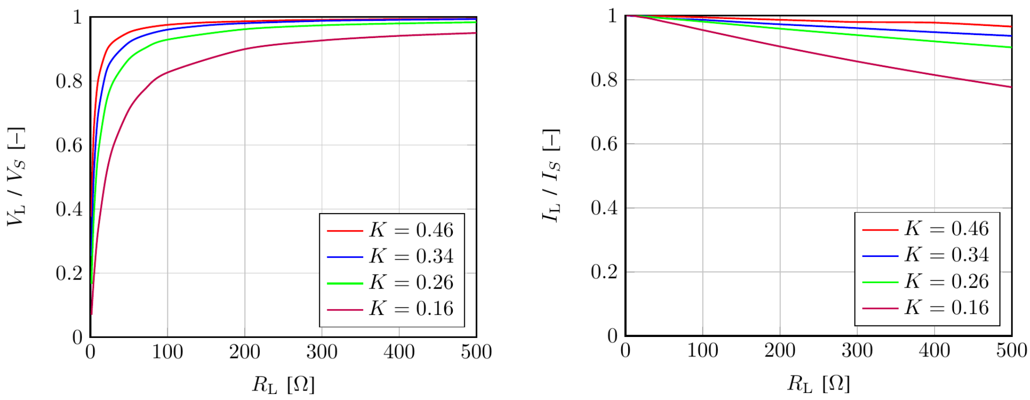

(a) Ratio of output to input voltage

(b) Ratio of output to input current

Figure 4.6: Simulation results for system performance variation due to coupling coefficient

4.3 EM simulations in practical conditions

In this section, we investigate the performance that assumes possible adverse effects when using the proposed method in a real environment. For the purpose of simplicity, we evaluate only by the simulation of the constant voltage design as $\alpha = 1$, $R_L = 100\Omega$ and other conditions are the same as in Table 4.1.

4.3.1 Impact of coupling coefficience

In the WPT application, the coupling coefficient between the transmitting and receiving coils is made as big as possible in order to improve the transmission efficiency. However, due to restrictions such as the use environment, the distance between the coils may be long, and applications where the coupling coefficient is not so large may be considered. Therefore, we investigate the difference in performance due to the changing coupling coefficient. Fig. 4.6 shows the results of the ratio of output to input voltage and current when the coupling coefficient is changed by varying the gap between the coils and the compensation circuit is mounted accordingly. It can be confirmed that the larger the coupling coefficient, the wider the stable range of the output.

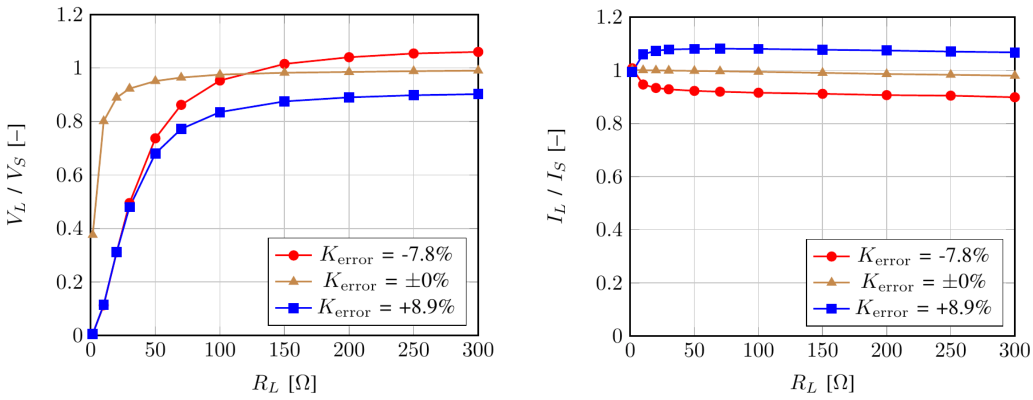

(a) Ratio of output to input voltage (b) Ratio of output to input current

Figure 4.7: Simulation results for Impact of deviation of coupling coefficient

4.3.2 Impact of deviation of coupling coefficient

Especially in dynamic WPT applications, the secondary side often moves irregularly. Since the coupling coefficient at the time of actual feeding is different from that at the time of system design, we investigate the influence of the deviation of the coupling coefficient on the proposed system.

Fig. 4.7 shows the results when when the coupling coefficient deviates by changing the distance between the coils from 20.0 mm at design to 17.5 mm and 22.5 mm. When error is compared with ± 0 %, the output voltage does not stabilize in the range where the load resistance is small for both positive and negative coupling coefficient deviations. In addition, when the coupling coefficient deviates to a negative value, the output voltage stabilizes at a large value with respect to the input voltage. On the other hand, a positive deviation stabilizes at a small value.

4.3.3 Impact of internal resistances

We have investigated the impact of internal resistances on the proposed system [31]. In [31], when the internal resistances of the transmitting and receiving coils are negligibly small, load-independent constant voltage functionality can be achieved. On the other hand, when the internal resistance is not negligible, the output voltage is not stabilized unless the load is sufficiently large. In this section, We investigate the performance of

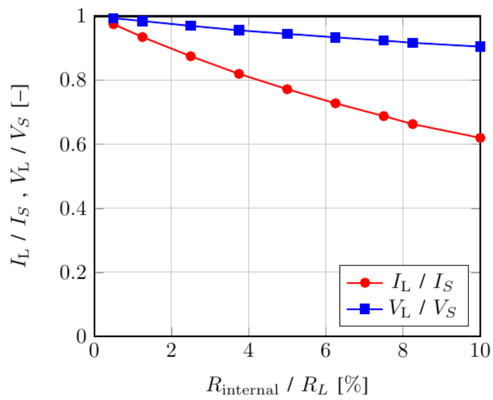

Figure 4.8: Simulation results for Impact of internal resistances

not only voltage but also current when the load resistance R_L is fixed and the internal resistances of the transmitting and receiving coils are changed.

Fig. 4.8 demonstrates the the ratio of output to input voltage and current as a function of the ratio of the internal resistances $R_{internal}$ to the load resistance $R_L = 100\Omega$. By connecting two resistors in series with the transmitting and receiving coils to vary internal resistances of the coils in a pseudo manner. It can be confirmed that the current ratio is greatly affected by the internal resistance compared to the voltage ratio.

4.3.4 impact of compensation errors

In practical applications, it is very difficult to accurately measure the parameters of the transmitting and receiving coils and additionally the capacitor contains an error. Therefore, we investigate the impact of compensation errors on the system.

Fig. 4.9 shows the results of the ratio of output to input voltage and current when the capacitors of the compensation circuit are changed by $\pm 15\%$. According to this figure, among the three types of capacitors, the error of C_1 greatly affects the performance. On the other hand, the error of C_2 doesn't significantly affect performance.

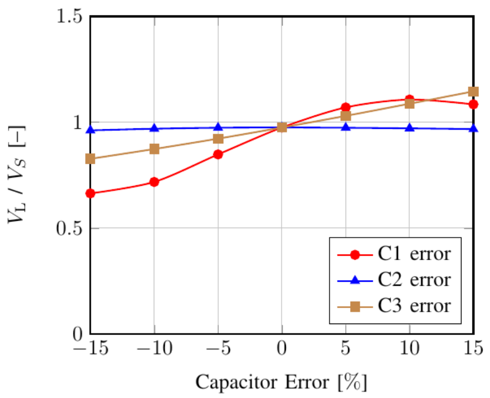

(a) Ratio of output to input voltage

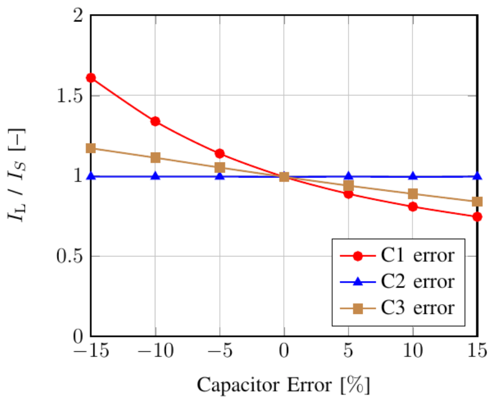

(b) Ratio of output to input current

Figure 4.9: Simulation results for impact of compensation errors

5 Experimental Evaluation

We investigate the availability of the design of the secondary-side compensation circuit mentioned in capter2 by experiment results.

5.1 Experiment setup

The experimental equipment consists of a DC power supply, a DC/AC inverter, transmitting and receiving coils, a compensation circuit, and a load resistance, as shown in Fig. 5.1. Both the transmitting and receiving coils are identical 2-layer and 10-turn each spiral coils made of litz wire with diameter of 0.08 mm (IWTX-4646BE-50). The operating frequency is set to 200 kHz. The observed values for self inductances of the transmitting and receiving coils are $L_1 = 23.89\ \mu$H and $L_2 = 23.62\ \mu$H, and their mutual inductance is $M = 11.69\ \mu$H. Other parameters are shown in Table 5.

5.2 Experiment results of constant voltage design

With these values, a compensation circuit is designed at $\alpha = 0.75, 1.0, 1.5$. The parameters of these compensation circuits and the input impedance of the system with a short load ($R_L = 0\ \Omega$) are shown in the TABLE 5.2. Reactive components of the system is canceled as well as simulation results.

Fig. 5.2 demonstrates the ratio of output to input voltage as function of the load resistance R_L. It was confirmed that the output voltage can be closer to the target value $V_L^\star = \alpha V_S$, and the smaller the value of α, the smaller the load value at which the stabilization starts.

Finally, Fig. 5.3 shows the waveform of input and output voltage at R_L of 110 Ω. It can be confirmed that the waveforms have the same tendency that the phase of

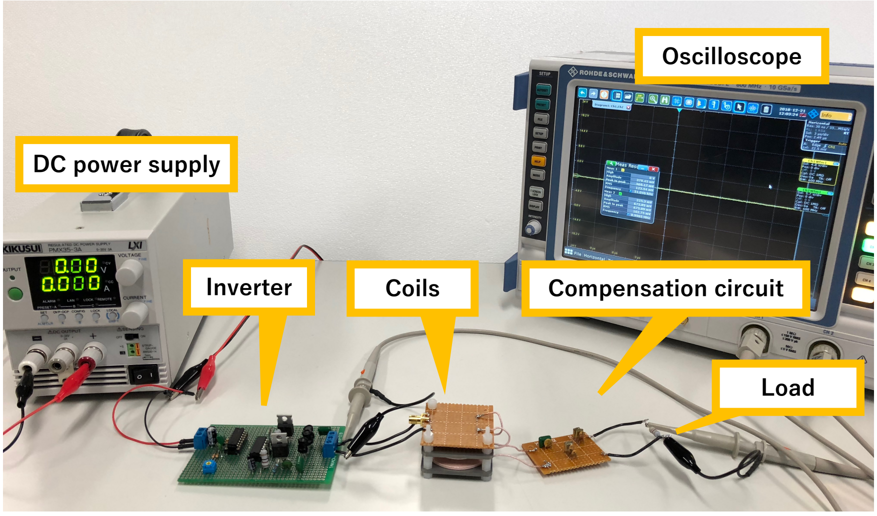

Figure 5.1: Experiment setup

output voltage are nearly identical to those of the input and the amplitude are close to $V_L^\star = \alpha V_S$ in any compensation circuit.

Table 5.1: Experiment paramters

Parameters	Value
Operating fequency f	200 [kHz]
Coil size	43×43 [mm]
Coil gap d	5.0 [mm]
Transmitting coil inductance L_1	23.89 [μH]
Internal resistance of transmitting coil r_1	272 [mΩ]
Receiving coil inductance L_2	23.62 [μH]
Internal resistance of receiving coil r_2	149 [mΩ]
Mutual inductance M	11.69 [μH]
Input voltage V_S	10 [V]

Table 5.2: Compensation circuit parameters of constant current design and input impedance of whole system in experiment

α	C_1	C_2	C_3	Z_{in}
1.5	103.95 [nF]	17.50 [nF]	36.21 [nF]	$2.0 + j0.6$ [Ω]
1.0	52.83 [nF]	51.74 [nF]	54.37 [nF]	$2.0 - j0.3$ [Ω]
0.75	44.37 [nF]	106.56 [nF]	67.54 [nF]	$2.2 + j0.5$ [Ω]

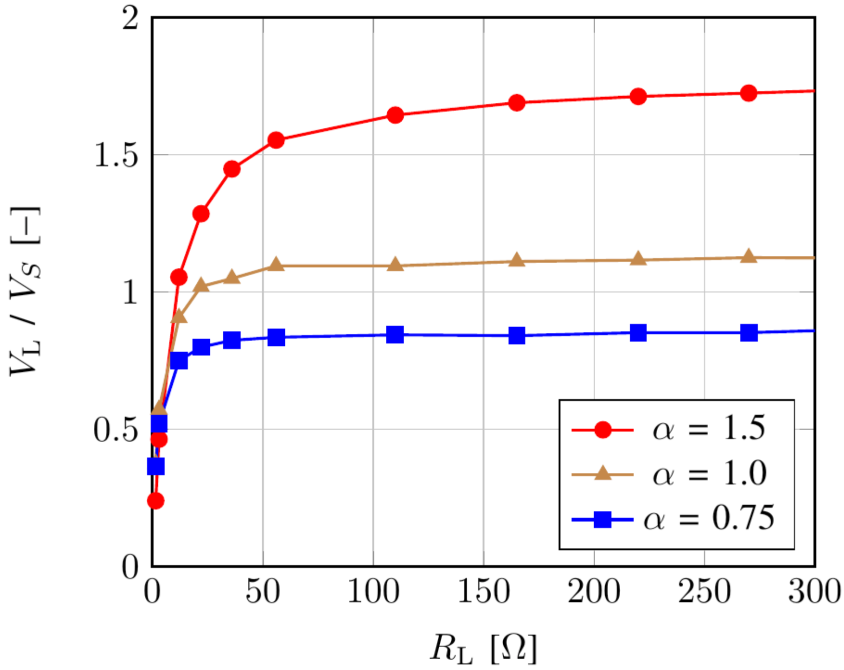

Figure 5.2: Experiment results for ratio of output to input voltage

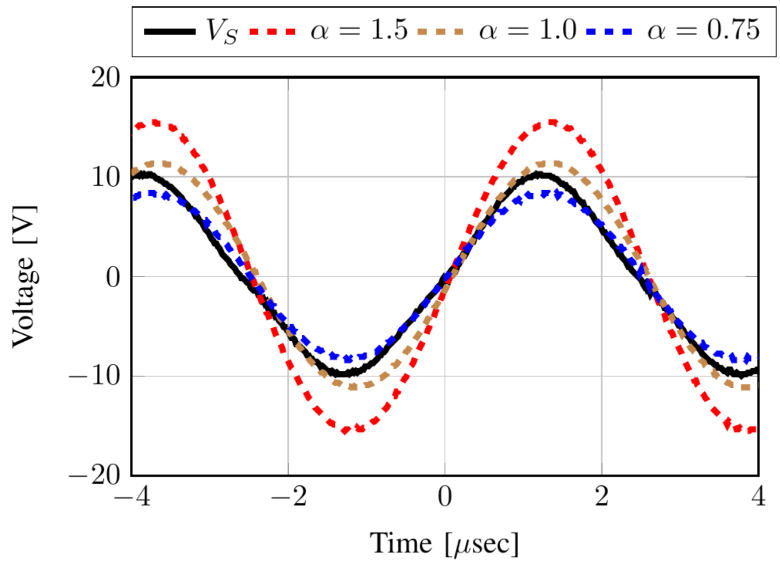

Figure 5.3: Experiment results for waveforms of input and output

6 Conclusion

In this thesis, we proposed the secondary-side compensation circuit for IPT system. First, we analyzed the design of the proposed method, and characteristics in practical conditions by using ABCD-parameters. Next, we then showed the effectiveness of the proposed method and the same tendency as the theoretical formula by simulation results. Finally, we confirmed the operation of the proposed system by experiments. From these results, we showed the operation and benefits of the secondary-side compensation circuit for IPT system, which was the purpose of this study. At the same time, we confirmed that this method can change the output freely and it is independent of the load value.

6.0.1 Future works

We verified only SISO (single-input single-output) IPT system with one transmitting coil and one receiving coil in this research. However, this method can simplefy the primary-side circuit. Therefore, this method is considered to have a great advantage in MISO (multiple-input single-output) and MIMO (multiple-input multiple-output) systems with multiple power transmission coils. In such a system, it is a future work to compare the efficiency with the conventional method.

Acknowledgements

I would like to thank Professor Minoru Okada for accepting and warmly welcoming me in his laboratory. He cared about my condition because I often stayed being at late night in my laboratory. His kindness and advice gave me a motivation to research. Also, I would like to express my thanks to all professors in my lab. Beside our labo meeting, they made time to discuss with me and provided me with useful advice from their knowledge and experience: Associate Professor Higashino Takeshi and remarkably Assistant Professor Quang-Thang Duong. He did carefully supervise me many times, and he gave me four chances to join international conference, and they are special experience for me. And, I want to express my thanks to Proffesor Hayashi Yuichi for his help about improving the quality of my master thesis. Thank to all the Network System lablatory members, I enjoyed having fun every day. Thank you all my freinds. I received a good stimulation from them. Finally, Thank you my family. I was able to spend peace of mind because my family supported me.

References

[1] “Wireless Power Demonstrated," https://thefutureofthings.com/5569-wireless-power-demonstrated/. (Accessed on 01/28/2020).

[2] G. A. Covic and J. T. Boys, “Inductive power transfer,” Proceedings of the IEEE, vol. 101, no. 6, pp. 1276–1289, June 2013.

[3] Manuel Pinuela, David C. Yates, Stepan Lucyszyn and Paul D. Mitcheson, “Maximising DC to Load Efficiency for Inductive Power Transfer,” IEEE Transactions on Power Electronics, vol. 28, no. 5, pp.2437-2447, May 2013.

[4] J. Shin, S. Shin, Y. Kim, S. Ahn, S. Lee, G. Jung, S. J. Jeon and D. H. Cho,“Design and Implementation of Shaped Magnetic-Resonance-Based Wireless Power Transfer System for Roadway-Powered Moving Electric Vehicles,” IEEE Trans. Ind. Electron., vol. 61, no. 3, pp. 1179-1192, March. 2014.

[5] S. Li and C. C. Mi,“Wireless Power Transfer for Electric Vehicle Application,” IEEE Trans. Emerg. Sel. Topics Power Electron., vol 3, pp. 4-17, no. 1, March. 2015.

[6] Y. Ko and Y. Jang,“The Optimal System Design of the Online Electric Vehicle Utilizing Wireless Power Transmission Technology,” IEEE Trans. Intell. Transp. Syst., vol 14, no. 3, pp. 1255-1265, Sept. 2013

[7] V. T. Nguyen, S. H. Kang, J. H. Choi and C. W. Jung,“Magnetic resonance wireless power transfer using three-coil system with single planar receiver for laptop applications,” IEEE Trans. Consum. Electron., vol. 61, no. 2, pp. 160-166, May. 2015.

[8] V. T. Nguyen, S. H. Kang and C. W. Jung,“Efficiency optimization of WPT system with a planar receiver for mobile applications”, WILEY Microwave and Optical Technology Letters, vol. 58, no. 8, pp. 1817-1819, Aug. 2016.

[9] A. Kamineni, M. J. Neath, A. Zaheer, G.A. Covic and J.T. Boys, “Interoperable EV detection for dynamic wireless charging with existing hardware and free resonance,” IEEE Trans. Transport. Electrific., vol. 3, pp. 370–379, June 2017.

[10] C. C. Mi, G. Buja, S. Y. Choi, and C. T. Rim, “Modern advances in wireless power transfer systems for roadway powered electric vehicles,” IEEE Trans. Ind. Electron., vol. 63, no. 10, pp. 6533–6545, Oct. 2016.

[11] W. Zhang and C. C. Mi, “Compensation topologies of high-power wireless power transfer systems,” IEEE Trans. Veh. Technol., vol. 64, no. 6, pp. 2261-2273, June 2015.

[12] A. Khaligh and S. Dusmez, “Comprehensive topological analysis of conductive and inductive charging solutions for plug-in electric vehicles,” IEEE Trans. Veh. Technol., vol.61, no. 8, pp. 3475-3489, Oct. 2012.

[13] H. I. Hsieh, T. H. Huang and S. F. Shih: “An inductive wireless charger for electric vehicle by using LLC resonance with matrix ferrite core group,” IEEE Applied Power Electronics Conference and Exposition (APEC), March 2015.

[14] S. Samanta, A. K. Rathore and S. Member: “A New Current-Fed CLC Transmitter and LC Receiver Topology for Inductive Wireless Power Transfer Application," Analysis, Design, and Experimental Results,” IEEE Trans. Transp. Electrif., vol. 1, no. 4, pp. 357-368, Sept. 2015.

[15] S. Li, W. Li, J. Deng, T. D. Nguyen and C. C. Mi: “A Double-Sided LCC Compensation Network and Its Tuning Method for Wireless Power Transfer,” Veh. Tech., vol 64, no. 6, pp. 2261-2273, Aug. 2014.

[16] Z. Pantic, S. Bai and S. M. Lukic, “ZCS LCC-compensated resonant inverter for inductive-power-transfer application,” IEEE Trans. Ind. Electron, vol 58, no 8, pp. 3500-3510, Sept. 2010.

[17] O. H. Stielau and G. A. Covic, “Design of loosely coupled inductive power transfer systems," Proc. Int. Conf. Power System Technology, vol. 1, pp. 85–90, Dec. 2000.

[18] A. J. Moradewicz and M. P. Kazmierkowski, “Contactless Energy Transfer System With FPGA-Controlled Resonant Converter," IEEE Transactions on Industrial Electronics, vol. 57, no. 9, pp. 3181-3190, Sept. 2010.

[19] M. H. Ameri, A. Y. Varjani and M. Mohamadian, “A New Maximum Inductive Power Transmission Capacity Tracking Method," Journal of Power Electronics, vol.16, no.6, pp.2202-2211, Nov. 2016.

[20] H. Li, J. Li, K. Wang, W. Chen and X. Yang, “A Maximum Efficiency Point Tracking Control Scheme for Wireless Power Transfer Systems Using Magnetic Resonant Coupling," IEEE Transactions on Power Electronics, vol. 30, no. 7, pp. 3998-4008, July 2015.

[21] R. Bosshard, J. W. Kolar, J. Mühlethaler, I. Stevanović, B. Wunsch and F. Canales, “Modeling and η-α-Pareto Optimization of Inductive Power Transfer Coils for Electric Vehicles," IEEE Journal of Emerging and Selected Topics in Power Electronics, vol. 3, no. 1, pp. 50-64, March 2015.

[22] R. Ota, N. Hoshi and J. Haruna, “Design of Compensation Capacitor in S/P Topology of Inductive Power Transfer System with Buck or Boost Converter on Secondary Side,” IEEJ Journal of Industry Applications, vol.4, no.4, pp. 476–485, 2015.

[23] Chwei-Sen Wang, O. H. Stielau and G. A. Covic, "Design considerations for a contactless electric vehicle battery charger," IEEE Transactions on Industrial Electronics, vol. 52, no. 5, pp. 1308-1314, Oct. 2005.

[24] R. Bosshard, U. Badstübner, J. W. Kolar and I. Stevanović, “Comparative evaluation of control methods for Inductive Power Transfer," 2012 International Conference on Renewable Energy Research and Applications (ICRERA), Nagasaki, pp. 1-6, 2012.

[25] Chwei-Sen Wang, O. H. Stielau and G. A. Covic, “Design considerations for a contactless electric vehicle battery charger," IEEE Transactions on Industrial Electronics, vol. 52, no. 5, pp. 1308-1314, Oct. 2005.

[26] M. Fu, Z. Tang and C. Ma, “Analysis and Optimized Design of Compensation Capacitors for a Megahertz WPT System Using Full-Bridge Rectifier," IEEE Transactions on Industrial Informatics, vol. 15, no. 1, pp. 95-104, Jan. 2019.

[27] W. Zhang, S. C. Wong, C. K. Tse and Q. Chen, “An Optimized Track Length in Roadway Inductive Power Transfer Systems," IEEE Journal of Emerging and Selected Topics in Power Electronics, vol. 2, no. 3, pp. 598-608, Sept. 2014.

[28] J. T. Boys, G. A. Covic and A. W. Green, “Stability and control of inductively coupled power transfer systems," Proc. IEEElect. Power Applicat., vol. 147, no. 1, pp. 37–43, Jan. 2000.

[29] B. L. Cannon, J. F. Hoburg, D. D. Stancil and S. C. Goldstein, “Magnetic Resonant Coupling As a Potential Means for Wireless Power Transfer to Multiple Small Receivers," IEEE Transactions on Power Electronics, vol. 24, no. 7, pp. 1819-1825, July 2009.

[30] H. Hong, D. Yang and S. Won, “The Analysis for Selecting Compensating Capacitances of Two-Coil Resonant Wireless Power Transfer System," 2017 IEEE International Conference on Energy Internet (ICEI), pp. 220-225, April 2017.

[31] Shogo Isogai, Quang-Thang Duong and Minoru Okada, “Impact of Internal Resistances on Performance of Receiver-side Compensation Circuit for Inductive Power Transfer Systems,” 2019 The International Workshop on Antenna Technology (iWAT 2109), Mar. 2019.

[32] Shogo Isogai, Quang-Thang Duong and Minoru Okada, “Receiver-side Compensation Circuits Based on T and Π equivalent models for Constant Voltage IPT,” 16th IEEE Asia Pacific Wireless Communications Symposium 2019 (APWCS2019), Aug. 2019.

Publication List

Domestic conference

[1] Shogo Isogai, Quang-Thang Duong and Minoru Okada, "Performance Evaluation of a Receiver-side Compensation Circuit for IPT Systems," IEICE Technical Committee on Wireless Power Transfer, Jan. 2019

International Conference

[2] Shogo Isogai, Quang-Thang Duong and Minoru Okada, "Impact of Internal Resistances on Performance of Receiver-side Compensation Circuit for Inductive Power Transfer Systems," 2019 The International Workshop on Antenna Technology (iWAT 2109), Mar. 2019

[3] Shogo Isogai, Quang-Thang Duong and Minoru Okada, "Receiver-side Compensation Circuits Based on T and Π equivalent models for Constant Voltage IPT," 16th IEEE Asia Pacific Wireless Communications Symposium 2019 (APWCS2019), Aug. 2019

[4] Shogo Isogai, Quang-Thang Duong and Minoru Okada, "Protecting Effect Against Unauthorized Receiver in IPT System with Secondary-Side Compensation Circuit," 2019 Asian Wireless Power Transfer Workshop (AWPT2019), Oct. 2019

[5] Shogo Isogai, Quang-Thang Duong and Minoru Okada, "A Constant Voltage Design for Inductive Power Transfer System with Multiple Loads," IEEE International Conference on Consumer Electronics 2020 (ICCE2020), Jan. 2020